MAUSAM

Assimilation of KOMPSAT-5 bending angle in GSI 4D-En Var assimilation system

SURYAKANTI DUTTA, V. S. PRASAD, FRANÇOIS VANDENBERGHE*,

HUI SHAO* and JAMES G. YOE**

National Centre for Medium Range Weather Forecasting, Noida, India

**Joint Center for Satellite Data Assimilation / University Corporation for*

Atmospheric Research (UCAR), Boulder, USA

***National Weather Service (NWS), College Park, USA*

(*Received 23 December 2021, Accepted 8 April 2024*)

e mail : suryakanti.dutta@gov.in

सार – कोरिया से बेंडिंग एंगल मल्टी-पर्पज सैटेलाइट - 5 (KOMPSAT-5) ग्लोबल नेविगेशन सैटेलाइट सिस्टम - रेडियो ऑक्लटेशन (GNSS-RO) डेटा को ग्लोबल डेटा आमेलन और पूर्वानुमान सिस्टम में समाहित किया जाता है।प्रेक्षणों को ग्रिड-पॉइंट स्टैटिस्टिकल इंटरपोलेशन (GSI) 4 डायमेंशनल - एन्सेम्बल वेरिएशनल (4D-EnVAR) विश्लेषण योजना का उपयोग करके शामिल किया गया । आमेलन से पहले, डेटा को संसाधित किया जाता है और COSMIC डेटा विश्लेषण और पुरालेख केंद्र (CDAAC), यूनिवर्सिटी कॉर्पोरेशन फॉर एटमॉस्फेरिक रिसर्च (UCAR) द्वारा गुणवत्ता नियंत्रण से गुजरना पड़ता है।इस अध्ययन में, मूल्यांकन और मूल्यांकन प्रक्रिया चार चरणों से गुजरती है: 1) कोल्ड स्टार्ट मोड में आमेलन के माध्यम से निदान; चक्रीय आमेलन के लिए2) ग्रीष्मकाल और 3) शीतकाल के महीनों और4) प्रचंड मौसम की घटनाओं पर इसके प्रभाव की जांच के लिए एक केस स्टडी ।दो अलग-अलग NWP पूर्वानुमान प्रयोग, नियंत्रण (CTRL नाम) और प्रयोग (KOMPSAT5 कहा जाता है), एक साथ चलाए जाते हैं। दोनों के बीच एकमात्र अंतर KOMPSAT-5 GNSS-RO की उपस्थिति (KOMPSAT5 में) और अनुपस्थिति (CTRL में) है। ग्रीष्मकालीन आँकड़े शीतकालीन की तुलना में बेहतर, महत्वपूर्ण और लगातार सुधार दिखाते हैं।

ABSTRACT. Bending Angle from Korea Multi-Purpose Satellite-5 (KOMPSAT-5) Global Navigation Satellite System - Radio Occultation (GNSS-RO) data is assimilated in the Global Data Assimilation and Forecast System. The observations are incorporated using the Grid-point Statistical Interpolation (GSI) 4 Dimensional - Ensemble Variational (4D-EnVAR) analysis scheme. Before assimilation, the data is processed and undergoes quality control by the COSMIC Data Analysis and Archive Center (CDAAC), University Corporation for Atmospheric Research (UCAR). In this study, the evaluation & assessment procedure goes through four phases : (*i*) diagnostics through assimilation in cold start mode; cyclic assimilation for (*ii*) summer and (*iii*) winter months and (*iv*) a case study for investigating its impact on severe weather events. Two separate NWP forecast experiments, a control (named CTRL) and the experiment (called KOMPSAT5), are run simultaneously. The only difference between the two is the presence (in KOMPSAT 5) and absence (in CTRL) of the KOMPSAT-5 GNSS-RO. Summer cycle statistics show better, significant, and consistent improvement compared to the winter cycle.

Key words – GNSS-RO, KOMPSAT-5, Assimilation, 4D-EnVAR.

1. Introduction

Global Navigation Satellite System - Radio Occultation, commonly referred to as GNSS-RO, functions using the radio waves transmitted from the Global Navigation Satellite Systems (GNSS) / Global Positioning System (GPS) satellites. The transmitted signal from the navigation satellites is received by a Low-Earth orbiting satellite during its setting or rising course relative to the transmitting satellite, thus, providing the radio occultation (RO) data (Ware *et al*., 1996). During its propagation from the transmitter to the receiver, the signal

passes through the Earth's atmosphere and undergoes refraction along its way. The bending angle is derived from the phase and amplitude of the dual L-band GPS signals (Jin *et al*., 2014). The magnitude of this refraction or bending depends upon the atmospheric density gradient, which in turn depends upon the water vapour concentration and temperature as functions of height in the atmosphere. This bending angle or refractivity also proves to be a good proxy of the water vapour content and temperature in the atmosphere.

GNSS-RO is very high-accuracy data (Kursinski *et al*., 1996; Rocken *et al*., 1997). In the past, there have been several studies investigating the potential impact of GNSS-RO onboard various platforms on weather prediction using numerical models (Liu *et al*., 2001; Poli and Joiner 2003; Zou *et al*., 2004, Wee and Kuo 2004; Cucurull *et al*., 2006; Cucurull *et al*., 2007; von Engeln *et al*., 2009). Significant error reduction in the temperature field is observed over the upper troposphere and lower stratosphere by Healy *et al*. (2005) when they assimilated the refractivity profiles into the United Kingdom Meteorological Office (UKMO/Met Office) weather model. Healy and Thépaut 2006 experimented with the bending angle soundings using the European Centre for Medium-Range Weather Forecasts (ECMWF) numerical model. They experienced a positive impact on the stratosphere over the Southern Hemisphere and at 100 hPa over the Tropics. The impact on regional model forecasts is highlighted through various studies (Wee *et al*., 2008; Chien *et al*., 2010; Zhou *et al*., 2014). Wee *et al*. (2008) assimilated GPSRO into the Fifth version of the National Center for Atmospheric Research Mesoscale Model (MM5) four-dimensional variational data assimilation system (4DVAR). They found improvement in the short-range forecasts over Antarctica. GNSS-RO data significantly improved the rainfall forecast valid at later model integration time (Chien *et al*. 2010). The impact of GNSS-RO was more significant when compared with that of drop windsonde. Zhou *et al*. (2014) demonstrated the effects of GPSRO refractivity data on the simulation of trade wind inversion and winter cold front. They assimilated the refractivity data using WRF-3DVar and found a better prediction of the trade wind inversion and the propagation of the cold front during the winter months. Numerous studies (Pommereau *et al*., 2007, Corti *et al*., 2008, Romps *et al*., 2009, Biondi *et al*., 2013, Rosado *et al*., 2018, Bai *et al*., 2020, Chen *et al*., 2020, Mueller *et al*., 2020) have proven the positive impact of GNSS-RO assimilation on cyclone forecasts and their usefulness in the study of various aspects of severe storms. Ruston *et al*., 2021 have shown that GNSS-RO from the COSMIC-2 mission impacts stratospheric temperature and wind fields over tropical regions.

Improvement was also observed in humidity fit to radiossondes and humidity-sensitive radiances over the tropical troposphere. Cucurull *et al*., 2021 have also found a significant impact on mass and wind fields globally.

Over recent years, there has been an increase in GNSS-RO data availability through commercial satellites, adding to the volume and quality of RO data available for research and operational activities. After proper validation and verification, these commercial satellites, mostly Cube Sats (Bowler, 2020), are accepted in various operational centres.

This study aims towards the assimilation of Korea Multi-Purpose Satellite - 5 (KOMPSAT-5) RO in the Global Data Assimilation and Forecast System. Here the Grid point Statistical Interpolation 4 Dimensional Ensemble Variational (GSI 4D-EnVar) analysis scheme (detailed in Wang *et al*., 2014; Kleist *et al*., 2015) is used for assimilation and the Global Forecast System (GFS) as the deterministic model. The resolution of the GSI cycles is T574 (Triangular truncation at wave number 574) and that of the GFS runs is T1534 (Triangular truncation at wave number 1534). The GSI system can assimilate the bending angle soundings and the refractivity profiles (Cucurull *et al*., 2007; Cucurull *et al*., 2008; Cucurull 2010) from RO observation. Presently, only the bending angle is assimilated. No thinning or superobbing is applied for RO assimilation. The bending angle forward operator, known as the National Centers for Environmental Prediction (NCEP) bending angle method (NBAM), developed by Cucurull *et al*., 2013, is used for assimilating GNSS-RO measurements in GSI. This method assimilates the bending angle, assuming the atmosphere to be spherically symmetrical. Bending angle derivation occurs before refractivity during the processing of radio occultation measurements. Cucurull *et al*. (2013) considered bending angle over refractivity as they are more robust to differences incorporated due to the difference in processing in different centres. Unlike refractivity, assimilation of bending angle does not require a climatological model and is free from negative biases found in the profiles over the atmosphere's super-refractive region. Assimilation of refractivity profiles ignores the horizontal gradient of refractivity in the atmosphere. The use of bending angles avoided the limitations caused due to this assumption. However, the higher variability of bending angle due to its height in the atmosphere makes their assimilation more complex and challenging. The local forward operator (NBAM) in GSI computes the total refractivity using the background information parameters (Cucurull *et al*., 2013). Total refractivity is derived using dry air & water vapour pressure, absolute temperature, atmospheric refractivity
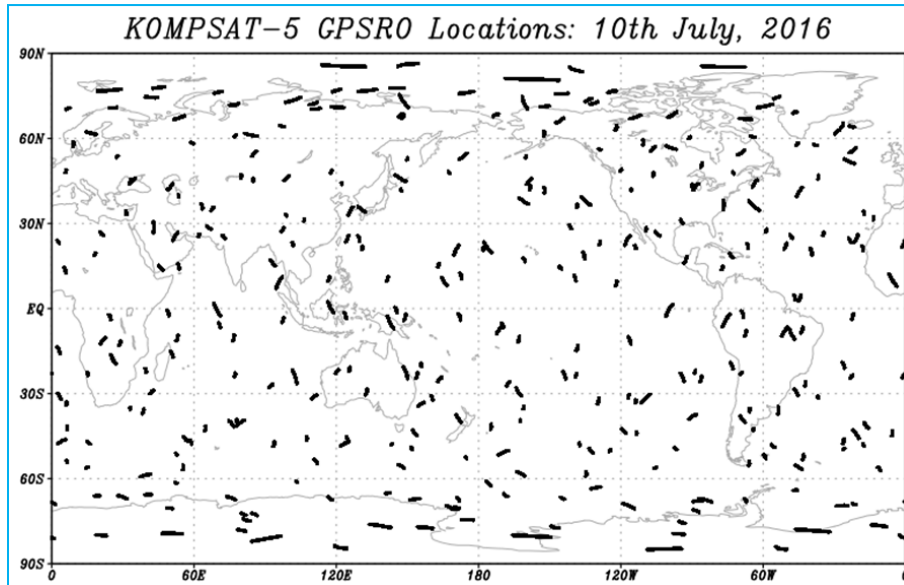
Fig. 1(a). Spatial Coverage of KOMPSAT-5 GPSRO on any arbitrary day
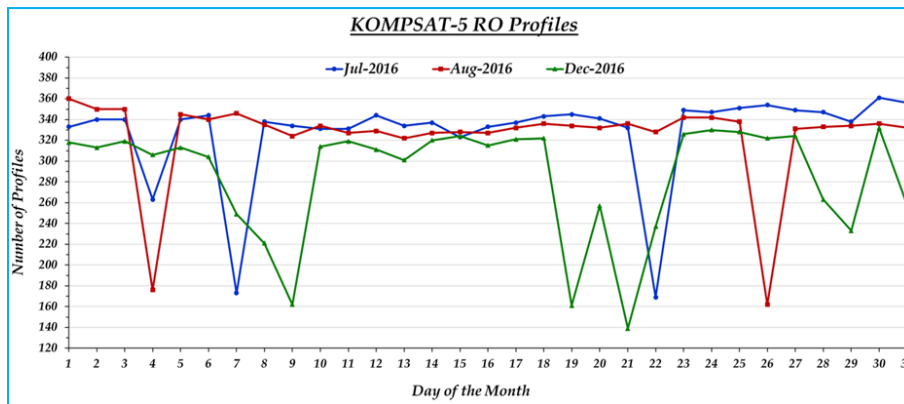

Fig. 1(b). Time series of number of KOMPSAT-5 GPSRO profiles

constants and the inverse compressibility factors. The bending angle is then simulated as a function of the impact parameter (a constant value for a particular ray) (Cucurull *et al.*, 2013) using the computed refractivity. The operational GSI assimilates the RO bending angle measured by the sensors onboard Constellation Observing System for Meteorology, Ionosphere, and Climate - 1 (COSMIC-1), METOP-A, METOP-B, TerraSAR-X and Tandem-X.

2. Data & methodology

The primary payload instrument on KOMPSAT5 is a Synthetic Aperture Radar (SAR) which provides information about Earth for geographic applications. The GNSSRO sensor, although a secondary payload instrument, nonetheless, provides valuable atmospheric observations. Aspace-borne integrated dual-frequency GPS receiver called the Integrated GPS Occultation Receiver (IGOR) is placed onboard KOMPSAT-5. It receives radio occultation (RO) signals and generates precision orbit determination (POD) data. The POD validation is performed by the onboard laser retro-reflector array (LRRA). KOMPSAT-5 is a sun-synchronous satellite with an average altitude of 550 km. It provides around 15 revolutions per day. Korea Astronomy and Space Science Institute (KASI) and the University Corporation for Atmospheric Research (UCAR) have developed the suite for near real-time data processing to generate KOMPSAT-5 GPSRO data, hereafter abbreviated as K5. The spatial coverage of K5 on any typical day is shown in Fig. 1(a). K5 has

comprehensive coverage distributed throughout the globe in a full daytime. Fig. 1(b) shows the time series of the number of K5 profiles available daily for July, August, and December 2016. The value ranges from as low as 139 profiles to as high as 361 profiles per day. Evaluation and assessment of K5 data for these three months are presented in this article.

The K5 data is processed and quality controlled by CDAAC (COSMIC Data Analysis and Archive Center), UCAR. Before being evaluated and assessed against the operational system, the K5 data quality is verified via an operational impact assessment. UCAR post-processed one month of bending angle from KOMPSAT-5 and COSMIC-1 RO. UCAR used this information for (*i*) analyzing and comparing quality control (QC) failure percentages for each QC failure mode of the retrieval process, and (*ii*) statistically comparing with ECMWF analysis for evaluating the error characteristics from the surface to 50 km altitude.

3. Results & discussions

The evaluation and assessment of the K5 bending angle are completed in four phases. In phase I, K5 is assessed through assimilation in cold start mode. This is followed by cyclic assimilation for a summer (phase II) and a winter month (phase III) and, a case study for investigating its impact on severe weather events (phase IV). The KOMPSAT-5 bending angle data after initial processing at UCAR were received starting from July-2016. So, July-2016 was opted for Phase-I of the assessment. This was followed by assessment of a summer month, *i.e.*, August-2016 and a winter month, which is December-2016.

3.1. *Phase-I : Assimilationin cold start mode*

In phase I, K5 is assimilated in cold-start mode for 00, 06, 12, and 18 UTC cycles for one month from 01-31 July 2016. Cold start mode helps investigate the model response to the observation and the observation quality. A 6-hour forecast from the operational GFS was accepted as the first guess for the GSI assimilation system (Wang *et al*., 2014; Kleist *et al*., 2015). The parameters concerning data usage *viz*. cross-validation parameter, gross error parameter, variational quality control parameter, the time interval for thinning, *etc*., are considered the same as that of COSMIC-FM6 [Flight Model 6, one of the COSMIC satellites/sensors]. The K5 data quality is evaluated in phase I against the COSMIC-1. Other operational RO observations are available, but COSMIC-1 was selected as both are processed by UCAR, and COSMIC-1 was already a well-established RO assimilated operationally (Cucurull *et al*., 2008).
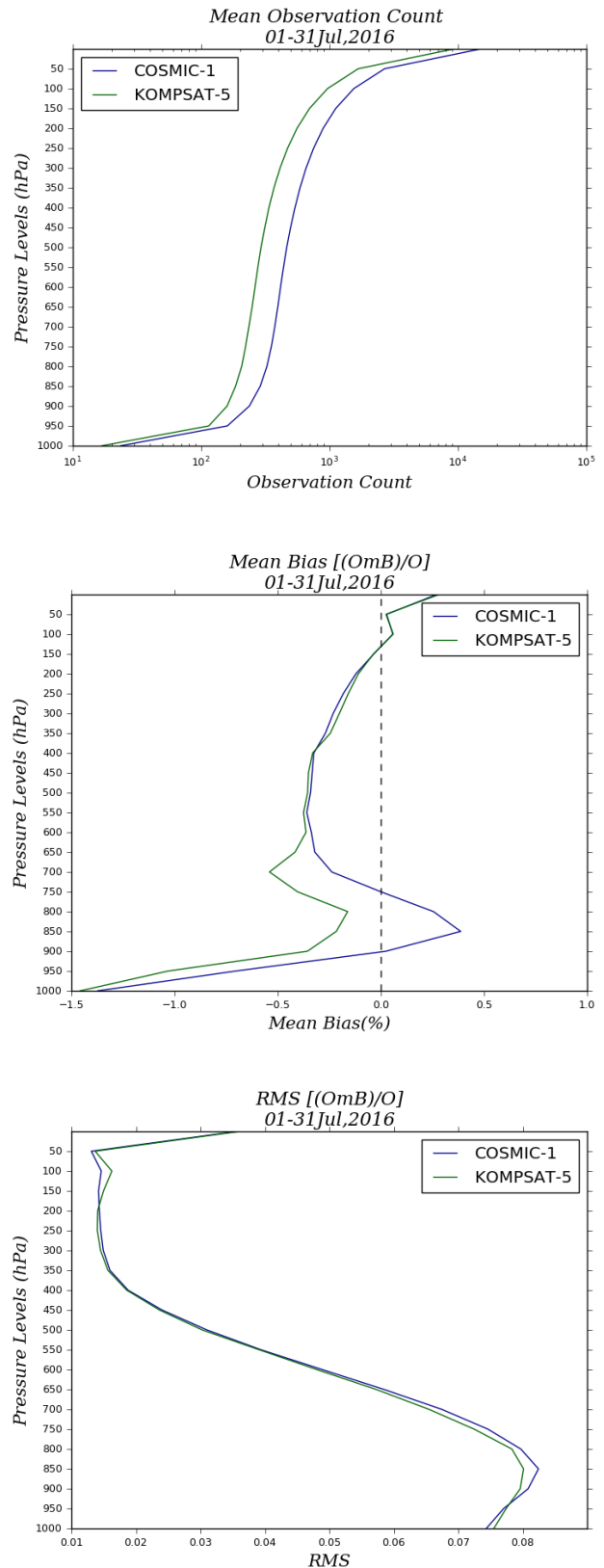
Fig. 2. Pre-Minimization Mean Diagnostics of July-2016 for the simulations in cold-start mode

The results are explained here as the Pre-Minimization (Fig. 2) and Post-minimization (Fig. 3) diagnostics. 'O' refers to the observations 'COSMIC-1' & 'KOMPSAT-5', 'B' is the model background, and 'A' is the model analyses. The plots provide a vertical profile of the quantitative estimates of mean observation count (upper panel), means of '(O-B)/O' & '(O-A)/O' in % (middle panel), and root mean square (RMS) of '(O-B)/O' & '(O-A)/O' (lower panel), respectively for the pre and post minimization results. It is to be noted that the runs in phase-I are cold-start where the first guess used from the operational runs does not have the influence of K5 observations. Radio occultation profiles have bending angle values retrieved over different pressure levels. So, the mean is computed over a layer of atmospheric thickness representing the mean diagnostic value for a pressure level, as demonstrated in Figs. 2&3. The diagnostics mean bias and RMS are values normalized with the observation (in this case, the bending angle). The pre-minimization plots (Fig. 2) are computed post-quality control (QC) of the dataset at the assimilation step. After quality control and before the beginning of the minimization procedure, the mean observation count of K5 is less than that of COSMIC-1 (Fig. 2, upper panel). This study uses only the setting occultation profiles for K5, as the rising profiles were unavailable for the experimentation period. Using only setting occultation limits the data count. The count increases with height and is maximum above 50 hPa. The pressure levels in these figures represent atmospheric layers of thickness of 50 hPa around the marked level. A drastic increase in mean observation values beyond the 50 hPa level is due to more data availability over higher altitudes and the fact that it includes all observations available beyond 50 hPa. The mean of (O-B)/O bias in the middle panel of Fig. 2 has a similar profile pattern for both the data. Close to the surface, K5 has a greater negative bias while, within 900 hPa to 750 hPa pressure level, COSMIC-1 has a positive mean bias (O-B)/O. Over higher levels, the values of mean bias converge and are similar for both observations.

In the lower panel of Fig. 2, the RMS of 'O-B/O' shows lower values for K5 within the pressure levels 900 - 650 hPa. Around 100 hPa K5 shows a slight increase in the pre-minimization RMS values. The bias and RMS change at post-minimization, seen in Fig. 3, where the middle and lower panels show the means (O-A)/O bias and RMS of (O-A)/O. The data with non-acceptable quality, with large biases and large differences compared to the background, are getting rejected from each profile. The differences incurred by these rejections are not visible in the mean observation count shown in Fig. 3 (upper panel) due to the plot's scale. However the effect of minimization is evident from the mean (O -A)/O
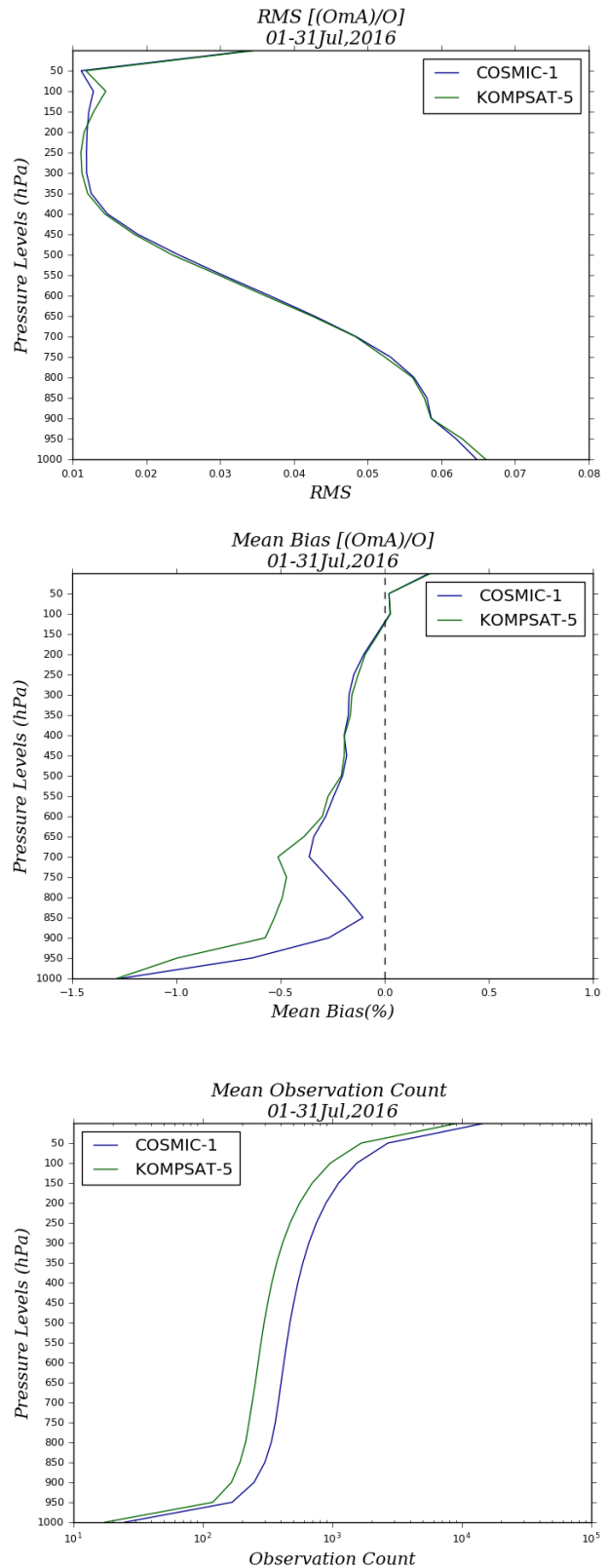
Fig. 3. Post-Minimization Mean Diagnostics of July-2016 for the simulations in cold-start mode
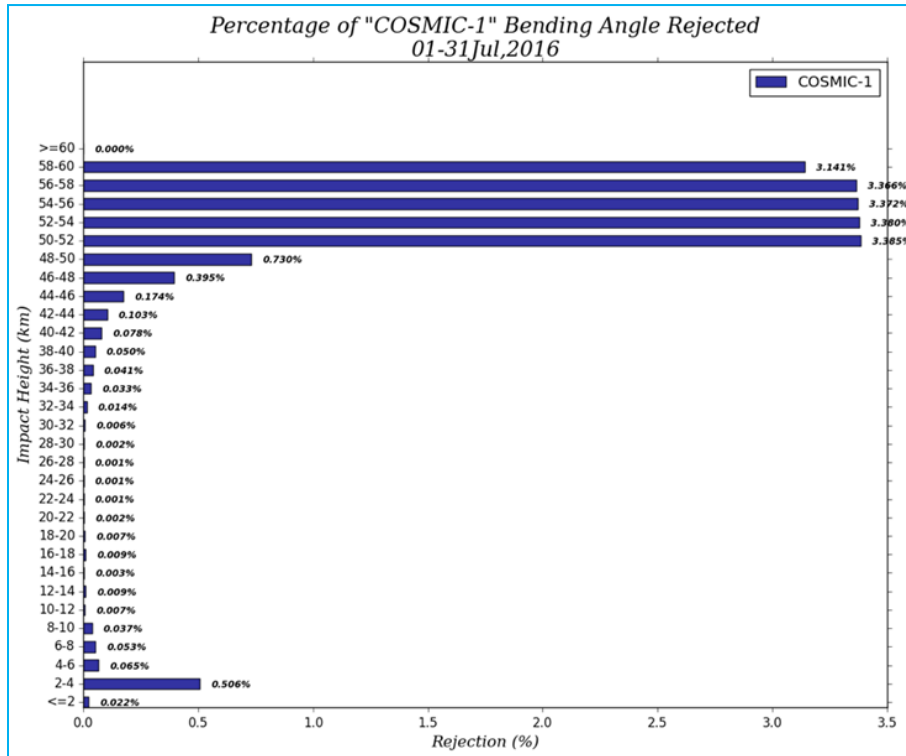
Fig. 4(a). Percentage of Total Data Rejection of COSMIC-1 during July-2016 for the simulations in cold-start mode
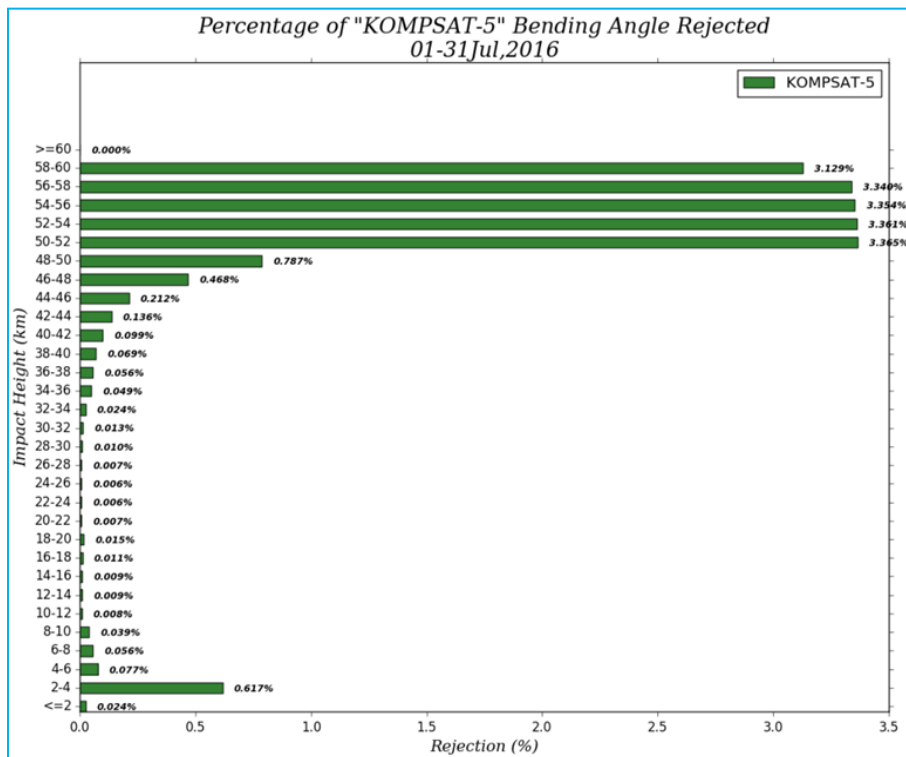
Fig. 4(b). Percentage of Total Data Rejection of KOMPSAT-5 during July-2016 for the simulations in cold-start mode
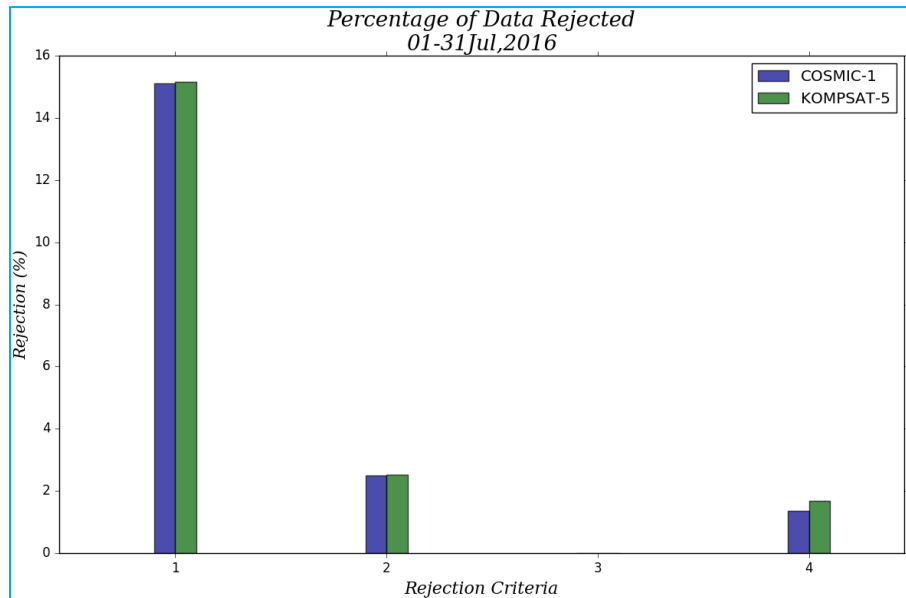
Fig. 5. Histograms depicting the Percentage of Data Rejected during July-2016 for the simulations in cold-start mode, based on the rejection criteria (1) Observation is outside the vertical boundary of the sigma levels. (2) Observation is at a height above 50 km. from the ground. (3) The ratio (Innovation Vector / Obs. Error) > Gross Error Parameter. (4) Observation close to or inside model SR(Super Refractivity) layer and/or (incremental bending angle > a cut-off value)

bias and RMS of (O-A)/O in the middle and lower panels of Fig. 3, respectively. At post-minimization, results show lowered bias and RMS values for both observations. The adjustment of values is more towards the lower to middle atmospheric levels. K5 has a larger negative bias (middle panel, Fig. 3) below the 500 hPa pressure level. The mismatch in RMS is close to the surface and upper levels where K5 continues to have higher values around 100 hPa. Close to the surface and around150-50 hPa, COSMIC-1 shows lower values of RMS. Proper assessment of any observation requires analysis of the rejected dataset. While investigating the rejected group's observations at post-minimization, Figs. 4(a&b) is generated, where the percentage of rejection is computed out of the total available data. Figs. 4(a&b) display the percentage of total data rejection of COSMIC-1 and KOMPSAT-5, respectively, for July 2016. The computation of rejection percentage is on the impact height layers of 2 km. thickness starting from the surface and extending to heights above 60 km. Impact height for a bending angle is the difference between the impact parameter and the local radius of curvature. For both datasets, maximum rejection occurs for impact heights greater than 50 km. Percentage of rejections below 4 km. impact height, though small, is higher for K5. Observations in the GSI get rejected due to four criteria, *viz.*, (*i*) Observation outside the vertical boundary of the NWP model; (*ii*) Observation at a height above 50 km. from the ground; (*iii*) The ratio (Innovation Vector / Obs.

Error) > Gross Error Parameter; and (*iv*) Observation close to or inside model SR (Super Refractivity) layer and/or (incremental bending angle > a cut-off value). Fig. 5 quantifies the rejection percentage due to each criterion, computed from the total observations available. In addition to the four rejection criteria described above, an additional rejection criterion is applied only to the Meteorological Operational Satellite (METOP) RO observations. All METOP RO observations below 8 km. impact height is rejected. Both observations show maximum rejection due to criterion 1. There is no rejection due to criterion 3. The rejection percentage due to criteria 1 & 2 is similar for COSMIC-1 and K5, whereas criterion-4 has more K5 rejected than COSMIC-1 RO.

Results from phase I provided the certainty of assimilating the K5 through cyclic assimilation for a longer duration, comprising two phases of summer and winter cycles. Each phase has two simulations; a CONTROL ('CTRL') and an experiment (called 'KOMPSAT 5'). The only difference between the two simulations is the presence of K5 RO in KOMPSAT5 and its absence in CTRL. GSI 4D-EnVar is the assimilation scheme (detailed in Wang *et al.*, 2014; Kleist *et al.*, 2015) used and GFS the forecast model. Six hourly assimilations were performed cyclically at 0000, 0600, 1200 and 1800 UTC. Forecasts up to 168 hours were prepared using GFS for every 0000 UTC initial condition. Like the cold start
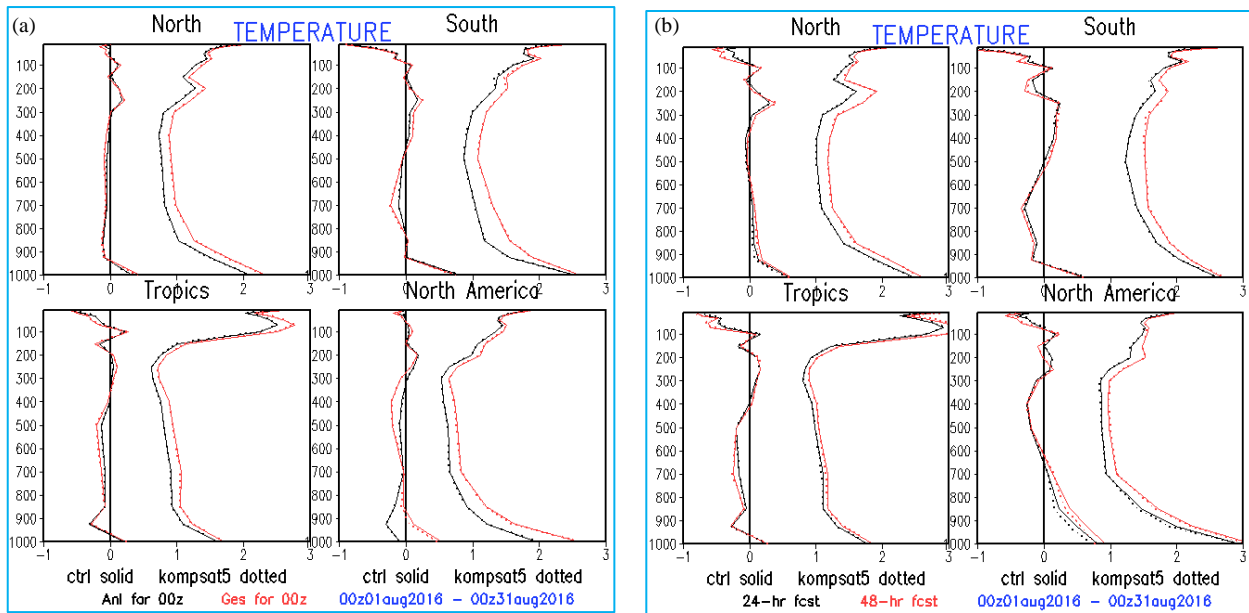
Figs. 6(a&b). Model (a) Analysis and First Guess & (b) 24 and 48-hour forecast, simulated temperature (degree Kelvin) fits to radiosonde observation
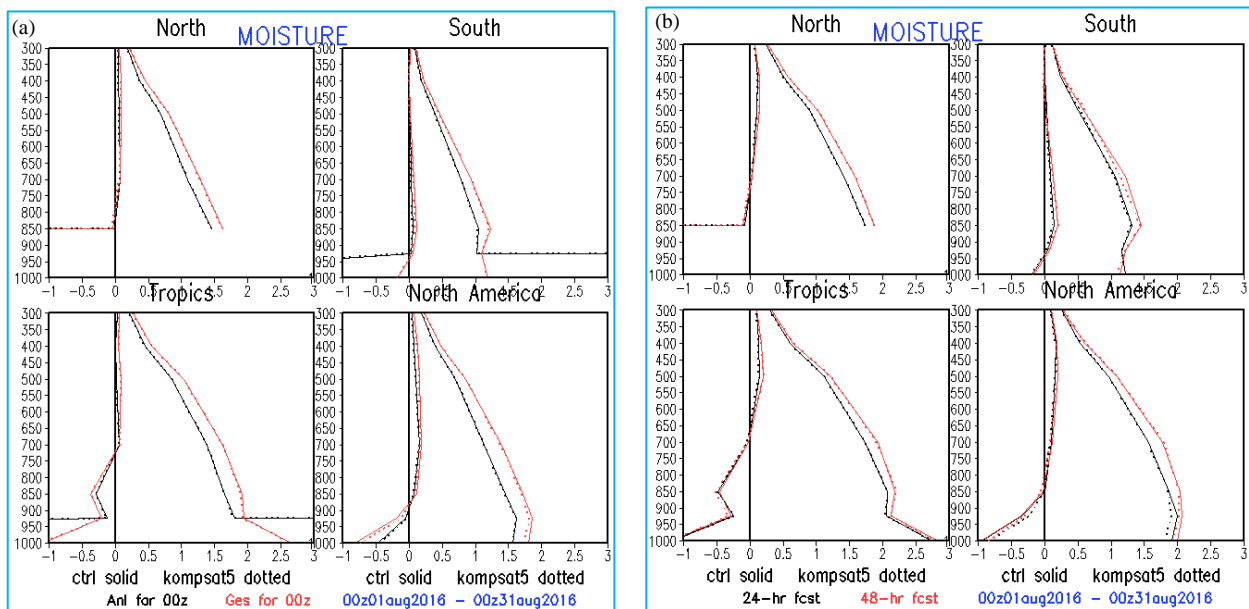
Figs. 7(a&b). Model (a) Analysis and First Guess & (b) 24 and 48-hour forecast, simulated moisture fits (relative humidity, %) to radiosonde observation

phase, in phases II and III, the parameter values concerning the assimilation of K5 are the same as COSMIC FM6.

3.2. *Phase-II : Simulation in Cyclic Mode - Summer Cycle*

In phase II, the assimilation of the K5 bending angle is evaluated for the summer month of August 2016. The assimilation is in a 6-hour cyclic mode. The regions referred to in the results are the Northern Hemisphere (NHX) : 20° - 80° N; the Southern Hemisphere (SHX): 20° - 80° S; the Tropics (TRO): 20° S - 20° N and the Pacific North America (PNA): 20° - 75° N, 180° - 320° E. The results shown are the monthly mean for August 2016.

3.2.1. *Model fits to observations*

Figs. 6-9 present the model simulated temperature, moisture, geopotential height, and wind fit to radiosonde
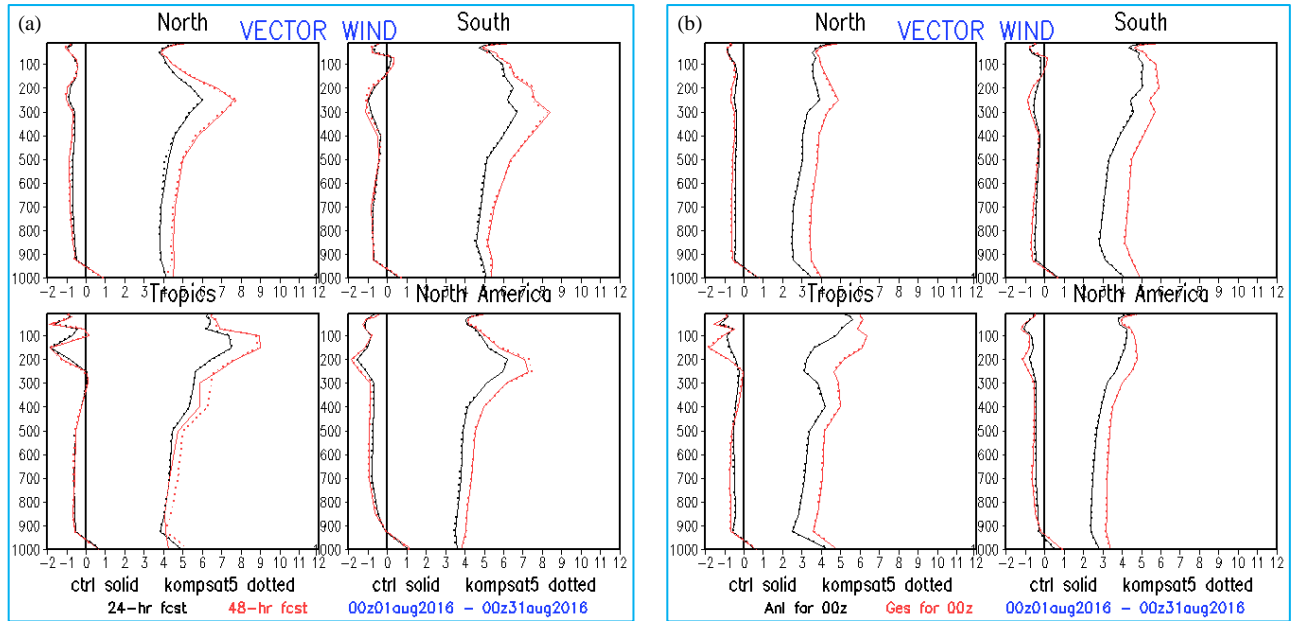
Figs. 8(a&b). Model (a) Analysis and First Guess & (b) 24 and 48-hour forecast, simulated vector wind fits to radiosonde observation
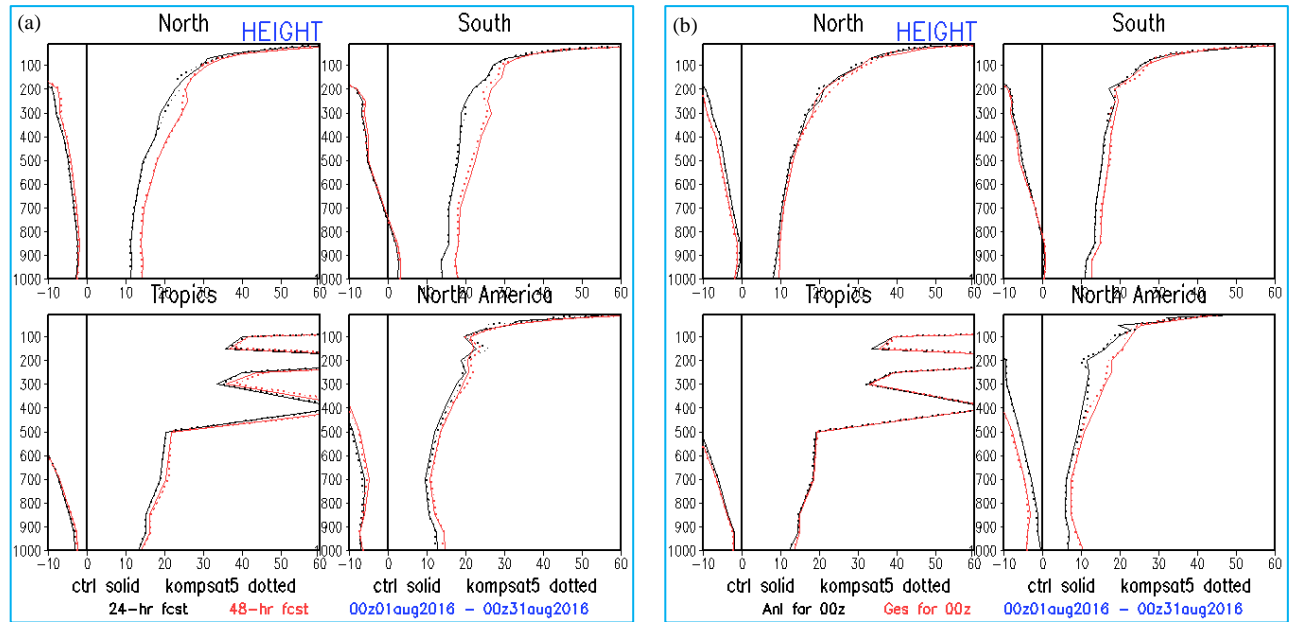
Figs. 9(a&b). Model (a) Analysis and First Guess & (b) 24 and 48-hour forecast, simulated geopotential (gpm) fits to radiosonde observation

observations. 'CTRL' simulation is represented by solid lines and 'KOMPSAT5' by dotted lines. The black lines are the analysis and 24-hour forecast, and the red lines are the first guess and the 48-hour forecast in sections (a) and (b), respectively. The parameters highlighted are bias and RMSE. For temperature (K) fits (Fig. 6), the control guess has a higher positive bias [Fig. 6(a)] in the lower atmosphere over North America. For the 24- & 48-hour

temperature forecast, the control has higher positive bias values from the lower to the middle atmosphere over the North American region [Fig. 6(b)]. Moisture (relative humidity, %) fits show similar results (Fig. 7). The control simulation has a higher positive bias for a 48-hour moisture forecast of the middle atmosphere over the southern hemisphere [Fig. 7(b)]. The vector wind fits to observation (Fig. 8) shows positive bias for 48- hour

Fig. 10. Scorecard for Forecast Verification statistics, computed against the ECMWF operational analyses for the month of August-2016
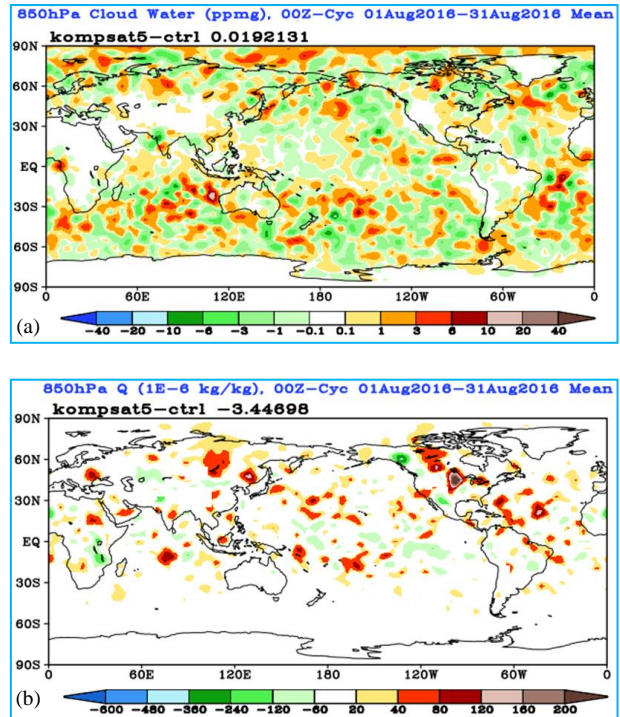
Figs. 11(a&b). (a) Surface Convective Available Potential Energy (J/Kg) analysis mean difference of 'KOMPSAT5 – CTRL' for the month of August-2016, (b) Surface Convective Inhibition (J/Kg) analysis mean difference of 'KOMPSAT5 – CTRL' for the month of August-2016


Figs. 12(a&b). (a) 850 hPa Cloud Water (ppmg) analysis mean difference of 'KOMPSAT5 – CTRL' over the month of August-2016, (b) 850 hPa Specific Humidity (1E-6 kg/kg) analysis mean difference of 'KOMPSAT5 - CTRL' over the month of August-2016

KOMPSAT5 forecast [Fig. 8(b)] from lower to upper atmosphere over the Tropics. Fig. 9 gives the geopotential height (gpm) fits to observation. There is a mismatch between the control and KOMPSAT5 for guess & analysis of the upper atmosphere over the northern hemisphere and North American region [Fig. 9(a)]. 24 & 48-hour forecast [Fig. 9(b)] shows similar behaviour. Over the southern hemisphere [Fig. 9(b)], control has a higher positive bias for geopotential fits from 48-hour forecasts.

3.2.2. *Forecast verification statistics*

The computation of forecast verification statistics (*viz.*, Anomaly Correlation, Root Mean Square Error - RMSE, Bias) is against the European Center for Medium - Range Weather Forecasts (ECMWF) operational analyses. Fig. 10 shows the scorecard summarizing the verification statistics results for forecasts valid for days 1, 3, 5 & 6.

The green colour & upward triangle imply that KOMPSAT5 is better, whereas the red colour and

downward triangle denote the CTRL to be better. The big and small triangles are, respectively, the significance at 99.9 & 99% confidence levels. The green and red coloured boxes mean significance at a 95% confidence level, whereas the differences with no statistical significance are grey. Geopotential height on higher layers and temperature on lower levels show significant improvement. There are instances of deterioration, as seen from the scorecard (Fig. 10). But the number of cases of significant improvement scores over the negative impact of K5 assimilation.

3.2.3. *Parameters affected due to assimilation of KOMPSAT-5 GPSRO*

Figs. 11&12 demonstrate some of the parameters affected due to the assimilation of K5. Fig. 11(a) shows the effect on Convective Available Potential Energy (CAPE) (J/Kg), and Fig. 11(b) highlights the impact on Convective Inhibition (CIN) (J/Kg). The mean difference between (KOMPSAT5 & CTRL) for CAPE is negative, and CIN is positive, indicating lesser atmospheric instability due to K5 assimilation. Figs. 12(a&b) show the impact on Cloud Water content (ppmg) and Specific
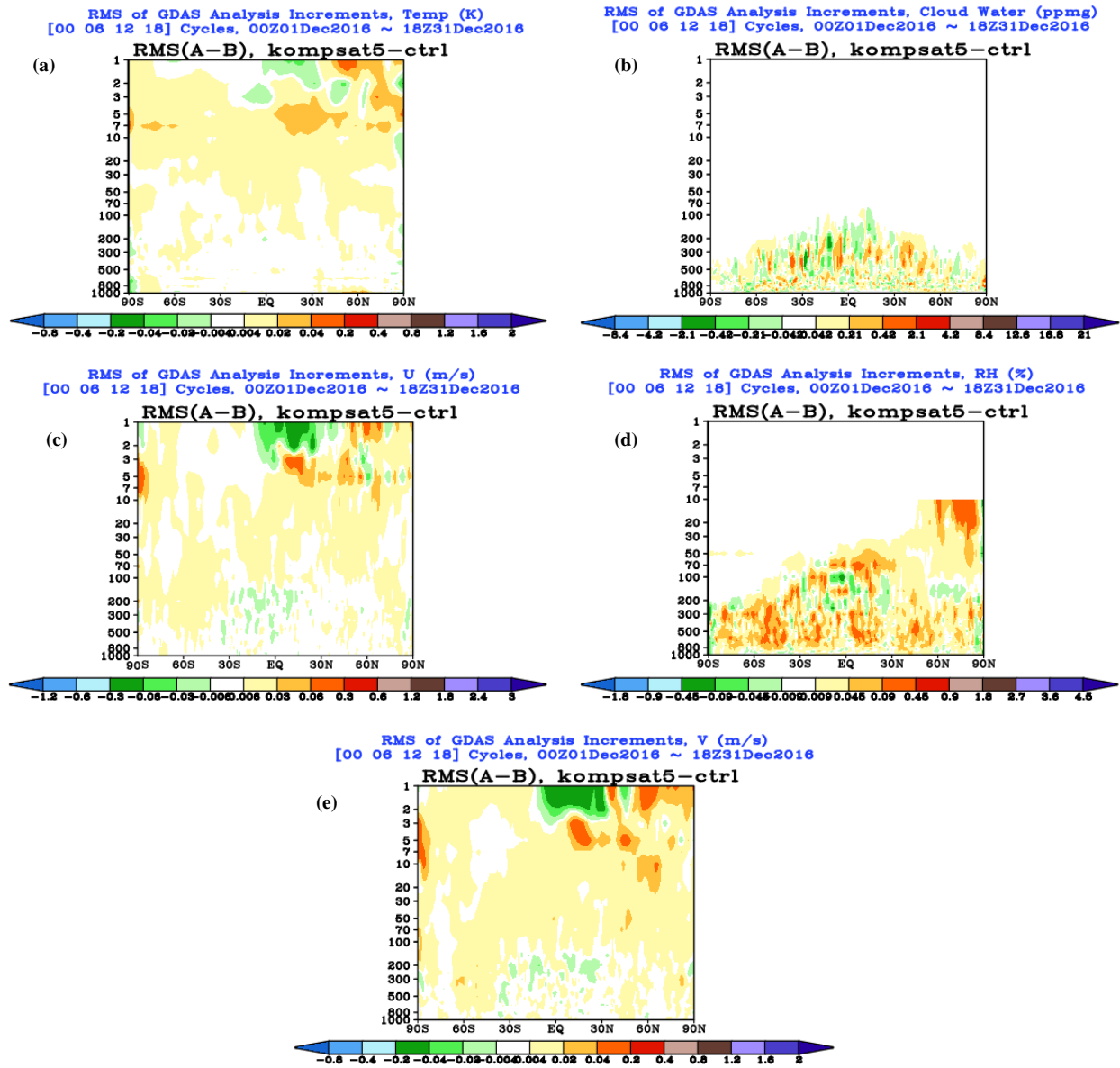
Figs. 13(a-e). Difference between RMS of Analyses Increments obtained from KOMPSAT5 and CTRL simulations for the zonal means of the parameters (a) Cloud Water (ppmg), (b) Temperature (K), (c) Relative Humidity (%), (d) Zonal Wind (m/s) and (e) Meridional Wind (m/s) profiles. ('A' implies Analysis and 'B' is the Background)

Humidity (kg/kg) for analysis at 850 hPa pressure level. The positive mean difference (KOMPSAT5 - CTRL) for cloud water shows an increase in cloud water content due to the assimilation of K5. Specific Humidity negative mean difference implies that K5 is influencing a drier atmosphere on model analysis at 850 hPa.

3.3. *Phase-III : Simulation in Cyclic Mode - Winter Cycle*

Phase III involves the assimilation of the K5 bending angle in the cyclic mode for the winter month of December 2016. The methodology for assimilation cycles, forecast simulation, and verification process remains precisely similar to the summer cycle.

3.3.1. *Analyses increments*

Figs. 13(a-e) depicts the Root Mean Square difference between analyses increments for the zonal mean of atmospheric parameters (*i*) Cloud Water, (*ii*) Temperature (T), (*iii*) Relative Humidity (RH), (*iv*) Zonal Wind component (U) and (*v*) Meridional Wind component (V). The cloud water adjustments [Fig. 13(a)]

			N. American				N. Hemisphere				S. Hemisphere				Tropics			
			Day 1	Day 3	Day 5	Day 6	Day 1	Day 3	Day 5	Day 6	Day 1	Day 3	Day 5	Day 6	Day 1	Day 3	Day 5	Day 6
Anomaly Correlation	Heights	250hPa																
		500hPa																
		700hPa																
		1000hPa					▲											
	Vector Wind	250hPa																
		500hPa																
		850hPa																
	Temp	250hPa																
		500hPa																
		850hPa																

EMC Verification Scorecard

Symbol Legend

▲	KOMPSAT5 is better than CTRL at the 99.9% significance level
▴	KOMPSAT5 is better than CTRL at the 99% significance level
(green)	KOMPSAT5 is better than CTRL at the 95% significance level
(grey)	No statistically significant difference between KOMPSAT5 and CTRL
(pink)	KOMPSAT5 is worse than CTRL at the 95% significance level
▾	KOMPSAT5 is worse than CTRL at the 99% significance level
▼	KOMPSAT5 is worse than CTRL at the 99.9% significance level
(blue)	Not statistically relevant

Start Date: 20161201

End Date: 20161231

Fig. 14. Scorecard for Forecast Verification statistics, computed against the ECMWF operational analyses for the month of December-2016
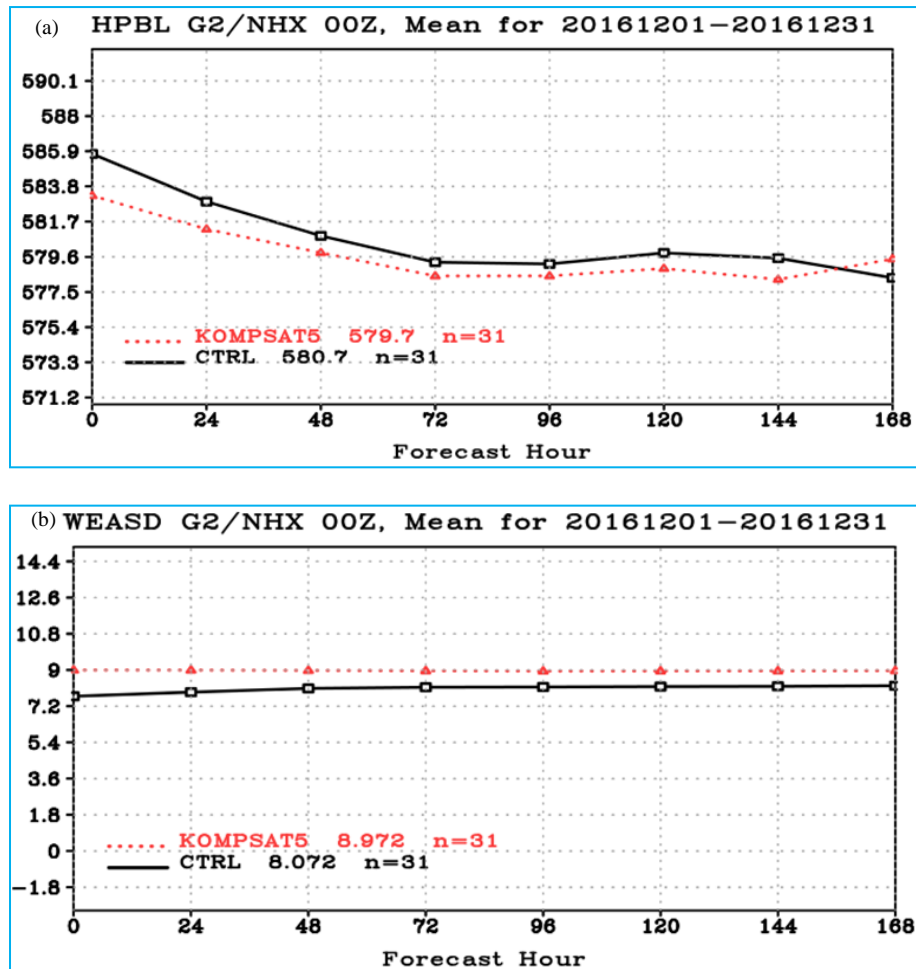
Figs. 15(a&b). Mean (a) Height of Planetary Boundary Layer (HPBL) and (b) Water Equivalent of Accumulated Snow Depth (WEASD) over the Northern Hemisphere for the forecast hours for the period 01 – 31 December 2016

in the troposphere are lower for the experimental simulation (KOMPSAT5) over the southern hemisphere (SH). For the relative humidity [Fig. 13(c)], this adjustment for KOMPSAT 5 is lower over the troposphere in SH and higher in upper atmospheric levels over the North Polar Region. The wind components, Zonal [Fig. 13(d)] and Meridional [Fig. 13(e)] and the temperature [Fig. 13(b)], show lower increment values for KOMPSAT 5 over the north tropical region and higher values over the north polar region in the upper atmospheric layers.

3.3.2. *Forecast verification statistics*

Fig. 14 highlights the forecast verification statistics for 01-31 December 2016 computed against the ECMWF operational analyses. Compared to summer statistics, significant improvement is not consistent for the winter cycle. One of the reasons could be the lesser number of KOMPSAT-5 RO profiles available and hence assimilated during December compared to the summer month of August 2016, as is seen in Fig. 1(b).

3.3.3. *Parameters affected due to assimilation of KOMPSAT-5 GPSRO*

In addition to the parameters discussed in Figs. 11&12, Fig. 15 highlights that assimilation of K5 also affects the parameters like the height of the planetary boundary layer (HPBL, Fig. 15(a) and water equivalent of accumulated snow depth (WEASD, Fig. 15(b). The region is Northern Hemisphere (NHX, 20° - 80° N) and the values are the temporal mean for the forecasts for the period 1st - 31st December 2016. Differences are consistent for all the forecast hours. KOMPSAT 5 generates larger WEASD and lower values of HPBL.
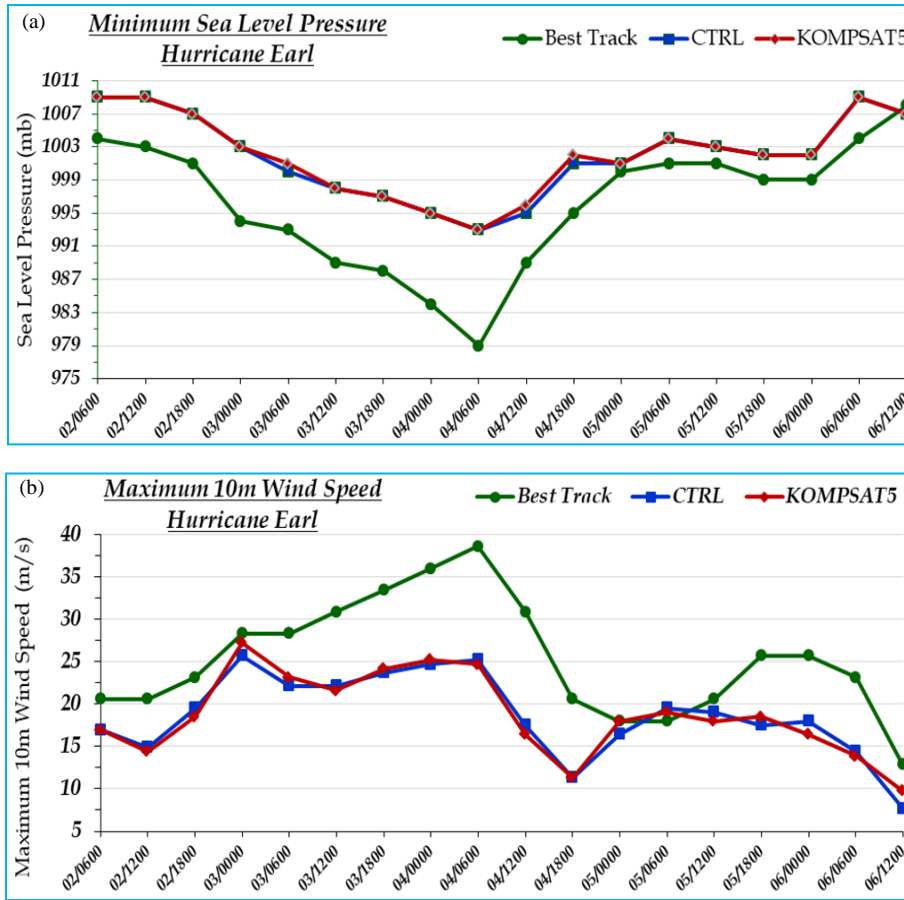
Figs. 16(a&b). (a) Minimum Sea Level Pressure & (b) Maximum 10m Wind Speed for Hurricane 'Earl'

The differences observed in the parameters discussed in section3 of phase - II & III do not confirm the forecast improvement but only imply how the NWP forecast model is reacting towards the assimilation of a new dataset, in this case, the KOMPSAT-5 bending angle data.

3.4. *Phase-IV : impact on severe weather events*

A case study on 'Earl,' a category-1 hurricane, was to visualize the impact of K5 on severe weather events. The life of 'Earl' was 2 - 6 August 2016. It made landfall in Belize and then crossed Guatemala and southern Mexico (Stewart 2017). Earl had an estimated peak intensity of 75 kt and a minimum central pressure of 979 mb. 6-hourly analyses are verified using the available Best Track information. Figs. 16(a&b) show the minimum sea-level pressure and maximum 10 m wind speed obtained from the 6-hourly assimilation cycles. Though the differences between the best track measurements and the simulated values are high, results from the control 'CTRL' and experimental simulation 'KOMPSAT-5' are close & similar in pattern. Fig. 17 provides the 6-hour analysis
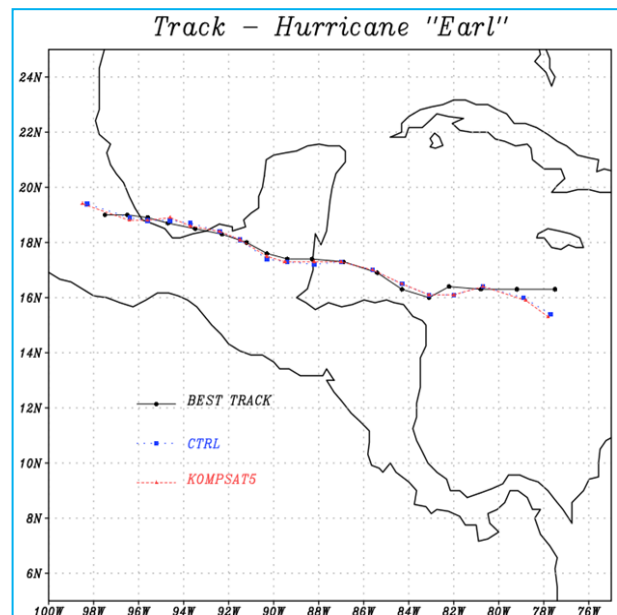
Fig. 17. Hurricane 'Earl' track as obtained from the 6-hourly analysis cycle
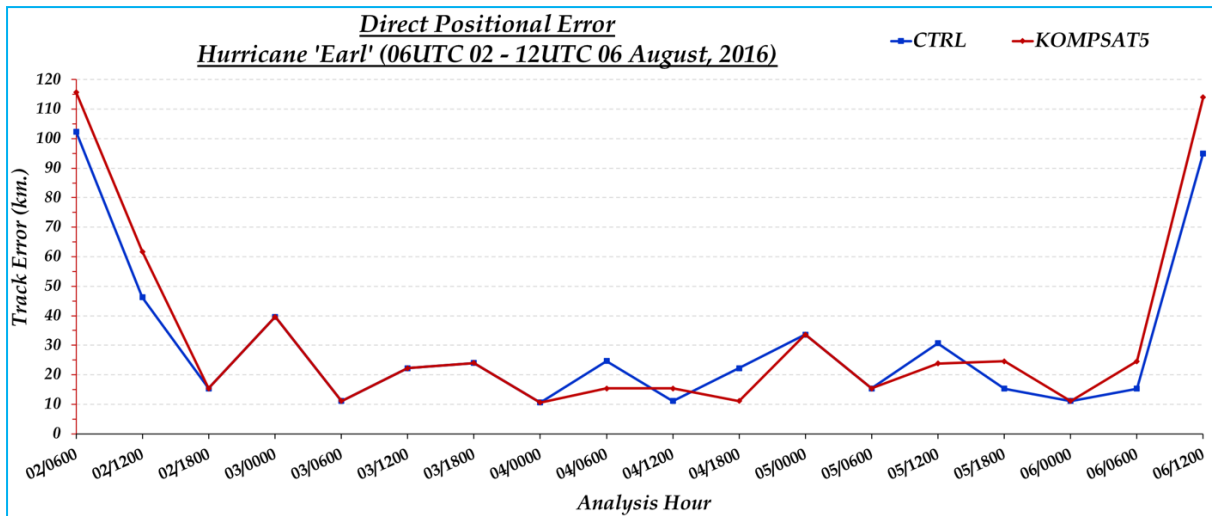
Fig. 18. Direct Positional Error (km) for Hurricane 'Earl' track as obtained from the 6-hourly analysis cycle of CTRL and KOMPSAT-5 simulations, computed against the available Best Track information

track compared with the best track measurements. Fig. 18 gives the quantitative comparison of the direct positional error (DPE) between the 6-hourly analysis from the CTRL and KOMPSAT 5 simulations. The computation of the error is using the available Best Track information. The DPE values from KOMPSAT 5 simulations are higher at the initiation and dissipation of the system. During the system's development and progress phase, the differences between the two DPEs are below 30 km. This being the only test case, an intense investigation involving a statistically acceptable number of cyclonic systems is required to conclude the influence of KOMPSAT-5 GPSRO on capturing tropical and extra-tropical cyclones.

4. Conclusion

The present study is an effort to assimilate KOMPSAT-5 GPSRO data in the Global Data Assimilation and Forecast System. This research work involving data assimilation in both cold start and cyclic mode and its impact on severe weather events has mixed results. However, the positive impact on various weather parameters, especially temperature and geopotential height is worth noting. The results represent values averaged for a month. Long-term continued use of the data could be beneficial for operational forecasts. In addition to temperature and geopotential height, assimilation of KOMPSAT-5 GPSRO also influenced parameters like specific humidity, cloud water, CAPE & CINE, the height of the planetary boundary layer, and water equivalent of accumulated snow depth. The only difference between the two setups (CTRL & KOMPSAT-

5) is the assimilation of KOMPSAT-5 bending angle data in the experimental run. The control run 'CTRL' does not contain the bending angle from KOMPSAT-5. Any noticeable difference between the two simulations is due to the KOMPSAT-5 bending angle observations used in this study.

The research work conducted used only the profiles received during the setting occultation. The future continuation of this work will involve studying the usability of the rising occultation profiles. It will require a more intensive study to assess the impact of K5 on severe weather events making the results statistically more robust.

Acknowledgement

Disclaimer : The contents and views expressed in this study are the views of the authors and do not necessarily reflect the views of the organizations they belong to

References

Bai, W., Deng, N., Sun, Y., Du, Q., Xia, J., Wang, X., Meng, X., Zhao, D., Liu, C., Tan, G., Liu, Z. and Liu, X., 2020, "Applications of GNSS-RO to Numerical Weather Prediction and Tropical

Cyclone Forecast", *Atmosphere*, **11**, 1204. doi : https://doi.org/10.3390/atmos11111204.

Biondi, R., Ho, S. P., Randel, W., Syndergaard, S. and Neubert, T., 2013, "Tropical cyclone cloud-top height and vertical temperature structure detection using GPS radio occultation measurements", *J. Geophys. Res.-Atmos.*, **118**, 5247-5259. doi : https://doi.org/10.1002/jgrd.50448.

Bowler, N. E., 2020, "An assessment of GNSS radio occultation data produced by Spire", *Q. J. R. Meteorol. Soc.*, **146**, 3772-3788.

Chen, S. Y., Kuo, Y. H. and Huang, C. Y., 2020, "The Impact of GPS RO Data on the Prediction of Tropical Cyclogenes is Using a Nonlocal Observation Operator: An Initial Assessment", *Mon. Wea. Rev.*, **148**, 7, 2701-2717.

Chien, F. C. and Kuo, Y. H., 2010, "Impact of FORMOSAT-3/COSMIC GPS radio occultation and dropwindsonde data on regional model predictions during the 2007 Mei-yu season", *GPS Solut.,* **14**, 51-63. doi : 10.1007/s10291-009-0143-2.

Corti, T., Luo, B. P., deReus, M., Brunner, D., Cairo, F., Mahoney, M. J., Matucci, G., Matthey, R., Mitev, V., Santos, F. H., Schiller, C., Shur, G., Sitnikov, N. M., Spelten, N., Vossing, H. J., Borrmann, S. and Peter, T., 2008, "Unprecedented evidence for over-shooting convection hydrating the tropical stratosphere", *Geo-phys. Res. Lett.*, **35**, L10810. doi :10.1029/2008GL033641.

Cucurull, L., 2010, "Improvement in the use of an operational constellation of GPS radio occultation receivers in weather forecasting", *Weather Forecasting*, **25**, 749-767. doi : 10.1175/2009WAF2222302.1.

Cucurull, L., Derber, J. C., Treadon, R. and Purser, R. J., 2007, "Assimilation of Global Positioning System Radio Occultation Observations into NCEP's Global Data Assimilation System", *Mon. Wea. Rev*., **135**, 3174-3193.

Cucurull, L. and Derber, J. C., 2008, "Operational Implementation of COSMIC Observations into NCEP's Global Data Assimilation System", *Weather Forecasting*, **23**, 702-711. doi : http://dx.doi.org/10.1175/2008WAF2007070.1.

Cucurull, L., Derber, J. C. and Purser, R. J., 2013, "A bending angle forward operator for global positioning system radio occultation measurements", *Journal of Geophys. Res.: Atmospheres*, **118**, 14-28. doi :10.1029/2012JD017782.

Cucurull, L., Kuo, Y. H., Barker, D. and Rizvi, S. R. H., 2006, "Assessing the impact of simulated COSMIC GPS radio occultation data on weather analysis over the Antarctic: A case study", *Mon. Wea. Rev*., **134**, 3283-3296.

Cucurull, L. and Casey, S. P. F., 2021, "Improved Impacts in Observing System Simulation Experiments of Radio Occultation Observations as a Result of Model and Data Assimilation Changes", *Mon. Wea. Rev*., **149**, 1, 207-220.

Engeln, A. V., Healy, S., Marquardt, C., Andres, Y. and Sancho, F., 2009, "Validation of Operational GRAS Radio Occultation Data", *Geophysical Research Letters*, **32**, L06815.

Healy, S. B., Jupp, A. M. and Marquardt, C., 2005, "Forecast impact experiment with GPS radio occultation measurements", *Geophys. Res. Lett*., **32**, L03804. doi : 10.1029/2004GL020806.

Healy, S. B. and Thépaut, J. N., 2006, "Assimilation experiments with CHAMP GPS radio occultation measurements", *Quart. J. Roy. Meteor. Soc*., **132**, 605-623.

Jin, S., Cardellach, E. and Xie, F., 2014, "GNSS Remote Sensing: Theory, Methods and Applications", *Springer*, London.

Kleist, D. T. and Ide, K., 2015, "An OSSE-based evaluation of hybrid variational-ensemble data assimilation for the NCEP GFS, Part II: 4D EnVar and hybrid variants", *Mon. Wea. Rev*., **143**, 452-470.

Kursinski, E. R., Hajj, G. A., Bertiger, W. I., Leroy, S. S., Meehan, T. K., Romans, L. J., Schofield, J. T., McCleese, D. J., Melbourne, W. G., Thornton, C. L., Yunck, T. P., Eyre, J. R. and Nagatani, R. N., 1996, "Initial results of radio occultation observations of Earth's atmosphere using the Global Positioning System", *Science*, **127**, 1107-1110.

Liu, H., Zou, X., Shao, H., Anthes, R., Chang, J., Tseng, J. H. and Wang, B., 2001, "Impact of 837 GPS/MET bending angle profiles on assimilation and forecasts for the period June 20-30, 1995", *J. Geophys. Res.*, **106**, 31771-31786.

Mueller, M. J., Kren, A. C., Cucurull, L., Casey, S. P. F., Hoffman, R. N., Atlas, R. and Peevey, T. R., 2020, "Impact of Refractivity Profiles from a Proposed GNSS-RO Constellation on Tropical Cyclone Forecasts in a Global Modeling System", *Mon. Wea. Rev*., **148**, 7, 3037-3057.

Pommereau, J. P. and Held, G., 2007, "Is there a stratospheric fountain?", *Atmos. Chem. Phys. Discuss*., **7**, 8933-8950.

Poli, P. and Joiner, J., 2003, "Assimilation experiments of one dimensional variational analyses with GPS/MET refractivity. In: Reigber C., Lühr H., Schwintzer P. (eds) First CHAMP Mission Results for Gravity, Magnetic and Atmospheric Studies", *Springer*, Berlin, Heidelberg. doi : https://doi.org/ 10.1007/978-3-540-38366-6_70

Rosado, K. and Chiao, S., 2018, "Assimilation of GPS Radio Occultation Data for Tropical Cyclogenesis : A Case Study in the Eastern Atlantic", *Open Atmospheric Sci. J.*, **12**, 33-47.

Ruston, B. and Healy, S., 2021, "Forecast Impact of FORMOSAT-7/COSMIC-2 GNSS Radio Occultation Measurements", *Atmospheric Science Letters*, **22**, e1019. doi : https://doi.org/ 10.1002/asl.1019.

Rocken, C., Anthes, R., Exner, M., Hunt, D., Sokolovskiy, S., Ware, R., Gorbunov, M., Schreiner, W., Feng, D., Herman, B. and Kuo, Y.-H., Zou, X., 1997, "Analysis and validation of GPS/MET data in the neutral atmosphere", *J. Geophys. Res*., **102**, D25, 29849-29866.

Romps, D. M. and Kuang, Z. M., 2009, "Overshooting convection in tropical cyclones", *Geophys. Res. Lett*., **36**, L09804. doi : https://doi.org/10.1029/2009GL037396.

Stewart, S. R., 2017, "Hurricane Earl (AL052016) 2-6 August 2016", National Hurricane Center Tropical Cyclone Report, 1-23.

Wang, X. and Lei, T., 2014, "GSI-Based Four-Dimensional Ensemble–Variational (4DEnsVar) Data Assimilation: Formulation and Single-Resolution Experiments with Real Data for NCEP Global Forecast System", *Mon. Wea. Rev*., **142**, 3303-3325.

Ware, R., Exner, M., Feng, D., Gorbunov, M., Hardy, K., Herman, B., Kuo, Y., Meehan, T., Melbourne, W., Rocken, C., Schreiner, W., Sokolovskiy, F., Solheim, F., Zou, X., Anthes, R., Businger, S. and Trenberth, K., 1996, "GPS Sounding of the Atmosphere from Low Earth Orbit: Preliminary Results", *Bull. Amer. Meteor. Soc.*, 77, 19-40.

Wee, T. K. and Kuo, Y. H., 2004, "Impact of a digital filter as a weak constraint in MM5 4DVAR: An observing system simulation experiment", *Mon. Wea. Rev*., **132**, 543-559.

Wee, T. K., Kuo, Y. H., Bromwich, D. H. and Monaghan, A. J., 2008, "Assimilation of GPS Radio Occultation Refractivity Data from CHAMP and SAC-C Missions over High Southern Latitudes with MM5 4DVAR", *Mon. Wea. Rev*., **136**, 2923-2944. doi : http://dx.doi.org/10.1175/2007MWR1925.1.

Zhou, C. and Chen, Y. L., 2014, "Assimilation of GPS RO Refractivity Data and Its Impact on Simulations of Trade Wind Inversion and a Winter Cold Front", *Nat. Sci*.,**6**, 605-614.

Zou, X., Liu, H., Anthers, R., Shao, H., Chang, J. and Zhu, Y. J., 2004, "Impact of CHAMP radio occultation observations on global analyses and forecasts in the absence of AMSU radiance data", *J. Meteor. Soc. Japan*, **82**, 533-549.